J|A|C|S
ARTICLES
Published on Web 04/15/2005

Phase Transition between Nanostructures of Titanate and Titanium Dioxides via Simple Wet-Chemical Reactions

H. Y. Zhu,*,† Y. Lan,†,‡ X. P. Gao,*,‡ S. P. Ringer,† Z. F. Zheng,†,‡ D. Y. Song,‡ and J. C. Zhao§

Contribution from the Australian Key Centre of Microanalysis & Microscopy and School of Chemistry, The University of Sydney, NSW 2006, Australia, Institute of New Energy Material Chemistry, Department of Material Chemistry, Nankai University, Tianjin 300071, China, and Institute of Chemistry, The Chinese Academy of Science, Beijing 100080, China

Received September 2, 2004; E-mail: h.zhu@emu.usyd.edu.au; xpgao@nankai.edu.cn

Abstract: Titanate nanofibers of various sizes and layered structure were prepared from inorganic titanium compounds by hydrothermal reactions. These fibers are different from "refractory" mineral substances because of their dimension, morphology, and significant large ratio of surface to volume, and, surprisingly, they are highly reactive. We found, for the first time, that phase transitions from the titanate nanostructures to TiO_2 polymorphs take place readily in simple wet-chemical processes at temperatures close to ambient temperature. In acidic aqueous dispersions, the fibers transform to anatase and rutile nanoparticles, respectively, but via different mechanisms. The titanate fibers prepared at lower hydrothermal temperatures transform to TiO_2 polymorphs at correspondingly lower temperatures because they are thinner, possess a larger surface area and more defects, and possess a less rigid crystal structure, resulting in lower stability. The transformations are reversible: in this case, the obtained TiO_2 nanocrystals reacted with concentrate NaOH solution, yielding hollow titanate nanotubes. Consequently, there are reversible transformation pathways for transitions between the titanates and the titanium dioxide polymorphs, via wet-chemical reactions at moderate temperatures. The significance of these findings arises because such transitions can be engineered to produce numerous delicate nanostructures under moderate conditions. To demonstrate the commercial application potential of these processes, we also report titanate and TiO_2 nanostructures synthesized directly from rutile minerals and industrial-grade rutiles by a new scheme of hydrometallurgical reactions.

I. Introduction

Titanates are well-known as functional ceramic materials (dielectric, piezoelectric, ferroelectric, and low absorption of infrared radiation),[1−4] and titanate-fibers (whiskers) are widely used as structural reinforcements in polymers, metals, and ceramic-composites[5,6] because of their outstanding mechanical properties and thermal stability. Moreover, titanium dioxide (TiO_2) is one of the most important metal-oxides.[7] In addition to its well-known use as pigments, these oxides have recently found advanced application as photocatalysts for degrading organic pollutants under ultraviolet irradiation, as catalyst supports,[8,9] as materials for converting solar energy into electricity, as gas sensors, and as Li ion battery materials.[7,10−13] There is also great interest in the development of titanates and TiO_2-based solids with nanoscale dimensions and high morphological specificity,[1−3,12−25] such as nanofibers,[13] nanosheets,[15,16]

† The University of Sydney.
‡ Nankai University.
§ The Chinese Academy of Science.

(1) Hennings, D.; Klee, M.; Waser, R. *Adv. Mater*. **1991**, *3*, 334−40.
(2) Newnham, R. E. *MRS Bull.* **1997**, *22*, 20−33.
(3) Rusina, O.; Eremenko, A.; Frank, G.; Strunk, H. P.; Kisch, H. *Angew. Chem., Int. Ed.* **2001**, *40*, 3993−3995.
(4) Urban, J. J.; Yun, W. S.; Gu, Q.; Park, H. *J. Am. Chem. Soc.* **2002**, *124*, 1186−1187.
(5) Yu, D.; Wu, J.; Zhou, L.; Xie, D.; Wu, S. *Compos. Sci. Technol*. **2000**, *60*, 499−508.
(6) Imai, T.; Nishida, Y.; Yamada, M.; Shirayanagi, I.; Matsubara, H. *J. Mater. Sci. Lett*. **1987**, *6*, 1257−1258.
(7) Fujishima, A.; Hashimoto, K.; Watanabe, T. *TiO_2 Photocatalysis Fundamentals and Applications*; BKC, Inc.: Tokyo, 1999.
(8) Chen, M. S.; Goodman, D. W. *Science* **2004**, *306*, 252−255.
(9) Stiehl, J. D.; Kim, T. S.; McClure, S. M.; Mullins, C. B. *J. Am. Chem. Soc.* **2004**, *126*, 13574−13575.
(10) Khan, S. U. M.; Shahry, M. A.; Ingler, W. B., Jr. *Science* **2002**, *297*, 2243−2245.
(11) Wagemaker, M.; Kentgens, A. P. M.; Mulder, F. M. *Nature* **2002**, *418*, 397−399.
(12) Kavan, L.; Kalbáč, M.; Zukalová, M.; Exnar, I.; Lorenzen, V.; Nesper, R.; Graetzel, M. *Chem. Mater*. **2004**, *16*, 477−485.
(13) Gao, X. P.; Zhu, H. Y.; Pan, G. L.; Ye, S. H.; Lan, Y.; Wu, F.; Song, D. Y. *J. Phys. Chem. B* **2004**, *108*, 2868−2872.
(14) Kim, Y. Il.; Salim, S.; Huq, M.; Mallouk, T. E. *J. Am. Chem. Soc.* **1991**, *113*, 9561−9563.
(15) Sasaki, T.; Watanabe, M.; Hashizume, H.; Yamada, H.; Nakazawa, H. *J. Am. Chem. Soc*. **1996**, *118*, 8329−8335.
(16) Sukpirom, N.; Lerner, M. M. *Chem. Mater*. **2001**, *13*, 2179−2185.
(17) Kasuga, T.; Hiramatsu, M.; Hoson, A.; Sekino, T.; Niihara, K. *Langmuir* **1998**, *14*, 3160−3163.
(18) Grätzel, M. *Nature* **2001**, *414*, 338−344.
(19) Linsebigler, A. L.; Lu, G.; Yates, J. T. *Chem. Rev*. **1995**, *95*, 735−758.
(20) Ma, R. Z.; Bando, Y.; Sasaki, T. *Chem. Phys. Lett*. **2004**, *380*, 577−582.
(21) Chen, Q.; Zhou, W.; Du, G.; Peng, L. M. *Adv. Mater*. **2002**, *14*, 1208−1211.
(22) Sun, X.; Li, Y. *Chem.-Eur. J*. **2003**, *9*, 2229−2238.
(23) Jung, J. H.; Kobayashi, H.; van Bommel, K. J. C.; Shinkai, S.; Shimizu, T. *Chem. Mater*. **2002**, *14*, 1445−1447.
(24) Yuan, Z. Y.; Zhou, W.; Su, B. L. *Chem. Commun.* **2002**, 1202−1203.
(25) Zhu, H. Y.; Gao, X. P.; Lan, Y.; Song, D. Y.; Xi, Y. X.; Zhao, J. C. *J. Am. Chem. Soc*. **2004**, *126*, 8380−8381.

10.1021/ja044689+ CCC: $30.25

and nanotubes[17] because of their demonstrated potential in solar energy conversion,[18] photocatalysis,[7,15,19,26,27] photovoltaic devices,[18,28,29] and carrier for metallic nanoparticles.[30,31] Moreover, these nanostructures have the potential to exhibit unusual properties and offer the opportunity to investigate physical and chemical processes in size-confined systems. The structure and resulting physical and chemical properties of these nanoparticles are size-dependent and cannot be determined by extrapolation of bulk characteristics.[32] For instance, TiO_2 and titanates are generally "refractory" mineral substances in bulk form and have good chemical and thermal stability.[3,14−16,33,34] Nonetheless, in the present study we find for the first time that phase transitions from the titanate nanostructures to TiO_2 polymorphs take place readily in wet-chemical processes at temperatures close to ambient. Furthermore, the resultant TiO_2 nanocrystals can react with concentrated NaOH solution, yielding hollow titanate nanotubes. This phase transition cycle is highly significant due to the fact that some of the transitions reported here have only been observed previously at very high temperatures,[7,15,16,33,34] and some could not even be achieved by pyrometallurgical processes.[25] Although the importance of continuing efforts to develop alternate approaches to synthesis of the nanostructures has been realized,[13−17,20−24] the potential for controlled reactions of these nanostructures has not drawn significant attention of researchers. In fact, phase transitions at moderate temperature are strongly preferred for constructing inorganic structures on nanometer scale[25] because the delicate nanostructures can easily be lost at high temperatures due to sintering. The present paper describes a reversible scheme of transitions between nanoscale titanium dioxides to and from nanoscale titanates.

II. Experimental Section

1. Sample Preparation. NaOH pellets and HNO_3 (both are AR grade and from Aldrich), and $TiOSO_4 \cdot xH_2O$ (98%, from Fluka) were used in the synthesis. Titanate nanofibers in this study were prepared via a hydrothermal reaction between a concentrate NaOH solution and an inorganic titanium salt.[25] Specifically, 10.7 g of $TiOSO_4 \cdot H_2O$ was dissolved into 80 mL of water and stirred until becoming clear. The resultant $TiOSO_4$ solution was mixed with a 100 mL of a 15 M NaOH solution while stirring. The mixture (white suspension) was then transferred into a 200-mL Teflon-lined stainless steel autoclave and kept at a temperature (T_h) between ambient and 200 °C for 48 h to yield titanate precipitates via a hydrothermal reaction. The white precipitate in the autoclaved mixture was recovered by centrifugation and washed with deionized water four times by dispersing the wet cake into 100 mL of water and recovering the solid by centrifugation. X-ray photoelectron spectroscopy (XPS) of the surface indicated that this washed product possessed a sodium content of ~10 wt % Na. This sodium titanate (Na-titanate) was then neutralized using 0.1 M HCl solution and washed with water to remove most of the sodium ions.

We dried the resultant hydrogen titanate (H-titanate) at 100 °C for 16 h and then dispersed this into a dilute (0.05 M) and concentrated (2.65 M) HNO_3 solution, respectively, at temperatures selected to first form anatase and rutile products as well as the intermediates of the phase transition. For phase transition experiments at temperature below 90 °C, aging was carried out with a water bath. Generally, a dispersion of 0.3 g of titanate and 30 mL of acid solution in a closes Pyrex glass bottle was shaken at the designated temperature for 48 h, while the phase transitions at higher temperature were carried out in autoclaves without shaking. Standard laboratory safety precautions, including the use of appropriate hoods, vessels, and safety gloves, were required when handling the strong acids and bases.

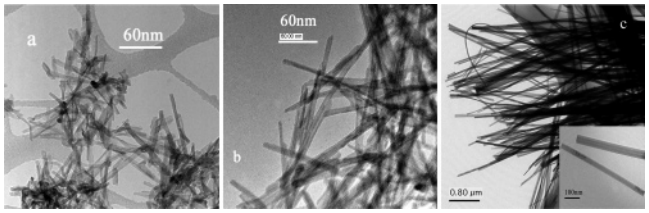

Figure 1. TEM images of the fibers. H-titanate fibers prepared by hydrothermal treatment at $T_h = 100$ °C (a), $T_h = 155$ °C (b), and $T_h = 200$ °C (c). As the hydrothermal temperature increases, the size and aspect ratio increase.

2. Sample Characterization. The microstructure and morphology of products were investigated using transmission electron microscopy (TEM) and X-ray diffraction (XRD) techniques. TEM images were recorded on a Philips CM12 TEM, employing an accelerating voltage of 120 kV. XRD patterns of the sample powders were recorded using a Shimadzu XRD-6000 diffractometer, equipped with a graphite monochromator. Cu Kα radiation ($\lambda = 1.5418$ Å) and a fixed power source (40 kV and 40 mA) were used. The samples were scanned at a rate of 1° (2θ)/min over a range of 2−80°, which covers the main characteristic diffraction peaks of the titanate, anatase, and rutile. Diffuse reflectance UV−visible reflectance (DR−UV−vis) spectra of the samples were recorded on a Varian Cary 5E UV−vis−NIR spectrophotometer. Nitrogen adsorption/desorption isotherms of the samples were obtained on a Quantachrome Autosorb-1 surface area and pore size analyzer; the samples were degassed at 150 °C in a vacuum below 10^{-3} Torr overnight prior to measurement. The specific surface area was calculated by the BET equation, using the data in a P/P_0 range between 0.05 and 0.2.

3. Photocatalytic Reaction. The UV source was a 100 W Hg lamp, the catalyst concentration was 0.05 g/L, and the starting concentration (C_0) of the synthetic dye surforhodamine (SRB) was 3×10^{-5} mol/L. Prior to irradiation, the dispersions in Pyrex glass vessels were magnetically stirred in the dark for ca. 30 min to secure the establishment of an adsorption/desorption equilibrium. At regular irradiation time intervals, the dispersion was sampled (4 mL), centrifuged, and subsequently filtered through a Millipore filter to separate the TiO_2 particles. The filtrates were analyzed by UV−vis spectra with a Shimadzu-160A spectrophotometer.

III. Results and Discussion

3.1. Titanate Fibers. Figure 1 provides a series of TEM images that summarize the results of synthesis of titanate nanofibers via an initial hydrothermal reaction between a caustic soda solution and an inorganic salt of titanium or titanium hydrate. As can be seen clearly from these TEM images of the hydrothermal reaction products, the hydrogen titanate (H-titanate) nanofibers of a high purity were obtained. In fact, the product of the hydrothermal reaction, prior to neutralizing with 0.1 M HCl solution, is sodium titanate (Na-titanate) nanofibers of the same morphologies shown in Figure 1. Neutralization with the dilute acid solution (the pH of the suspension in this step was 7 or above) yielded hydrogen titanate (H-titanate) nanofibers that retained the fibril morphology. The influence

(26) Zhang, M.; Jin, Z. S.; Zhang, J. W.; Guo, X. Y.; Yang, J. J.; Li, W.; Wang, X. D.; Zhang, Z. J. *J. Mol. Catal. A: Chem.* **2004**, *217*, 203−210.
(27) Yin, H. B.; Wada, Y.; Kitamura, T.; Kambe, S.; Murasawa, S.; Mori, H.; Sakata, T.; Yanagida, S. *J. Mater. Chem.* **2001**, *11*, 1694−1703.
(28) Sugiura, T.; Yoshida, T.; Minoura, H. *Electrochem. Solid-State Lett.* **1998**, *1*, 175−177.
(29) Tokudome, H.; Miyauchi, M. *Chem. Commun.* **2004**, 958−959.
(30) Ma, R. Z.; Sasaki, T.; Bando, Y. *J. Am. Chem. Soc.* **2004**, *126*, 10382−10388.
(31) Huang, J. G.; Kunitake, T.; Onoue, S. Y. *Chem. Commun*. **2004**, 1008−1009.
(32) Steigerwald, M. L.; Brus, L. E. *Acc. Chem. Res.* **1990**, *23*, 183−188.
(33) Andersson, S.; Wadsley, A. D. *Acta Crystallogr.* **1962**, *15*, 194−201.
(34) Sasaki, T.; Nakano, S.; Yamauchi, S.; Watanabe, M. *Chem. Mater*. **1997**, *9*, 602−608.

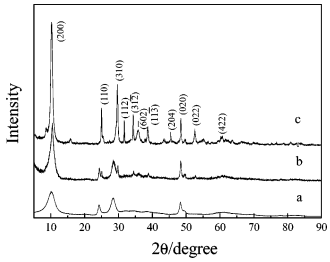

Figure 2. X-ray diffraction (XRD) patterns of the samples. From the bottom: trace *a* is for the fibers shown in Figure 1a, trace *b* is for the fibers in Figure 1b, and trace *c* is for the long fibers in Figure 1c. The diffraction peak became sharper as the temperature T_h in the synthesis increases.

of the experimental parameters of the wet-chemical reactions on the morphology and crystallinity of the product nanostructures is considerable and, in the case of the product H-titanate nanofibers, was observed to be most sensitive to the temperature of the hydrothermal treatment, T_h (Figure 1). Linear fibers ~30−60 nm long and 3−5 nm thick formed at 100 °C or below (Figure 1a), and the BET specific surface area of these fibers is 346 m^2/g. Fibers of 100−200 nm length and 8−10 nm width (Figure 1b) were obtained at a temperature between 130 and 155 °C. The sample prepared at 155 °C had a BET specific surface area of 302 m^2/g. Further increase in the reaction temperature resulted in the formation of remarkably long fibers. These straight fibers were 40−80 nm thick and up to 30 μm long, with an aspect ratio over 200 (Figure 1c). The BET specific surface area of this sample was very low at 27 m^2/g. We also observed that the degree of crystallinity of these fibers increases with increasing temperature T_h as illustrated by the XRD patterns of the samples (Figure 2). At a lower T_h, the diffraction peaks in the XRD pattern were broader, reflecting a poorer crystallinity of the sample prepared at a lower temperature.

According to the XRD traces, the long fibers obtained at T_h = 200 °C represent a relatively well-crystallized layered titanate (Figure 2). The XRD results from the fibers are similar to that of the layered titanate $H_2Ti_3O_7 \cdot xH_2O$ with a monoclinic lattice (*C*2/*m*).[34,35] This is consistent with the fact that titanate structures have TiO_6-octahedra as the basic structural units[14−16,33,34,36] such that each TiO_6 octahedron shares edges with other octahedra so as to form a zigzag chainlike structure. These chains join together by sharing edges to form layers and Na^+ ions or protons exist between the layers.[33] The distance between the layers is variable,[15,36] and this explains the flexibility of the long fibers (Figure 1c). We observed many curved fibers, and the product solid is cotton-like, soft with resiliency, and has a low apparent density. With this wet-chemical approach, one could readily achieve titanate nanofibers on multiple length-scales and exert control on their size and crystallinity by adjusting the temperature of hydrothermal treatment, T_h. The significance of these findings can be understood in terms of the fact that titanates are usually prepared by heating a mixture of alkali carbonate and titanium dioxide at temperatures above 800 °C.[1−6,14−16,33,34,36] Due to the pyrometallurgical nature of this reaction, the sintering effect produces large titanate particles, having a spheroidal morphology of several micrometers in diameter.

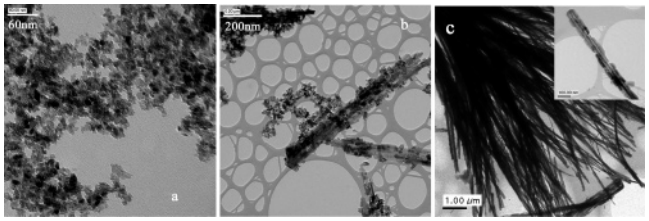

Figure 3. TEM images of anatase products of the phase transition reactions that H-titanate fibers reacted with 0.05 M HNO_3 at different temperature. (a) Monodispersed anatase nanocrystals obtained at 80 °C from the H-titanate fibers in Figure 1a. (b) Aggregates of anatase nanocrystals obtained at 120 °C from the H-titanate fibers in Figure 1b. (c) Anatase aggregates formed at 120 °C from the long H-titanate fibers in Figure 1c.

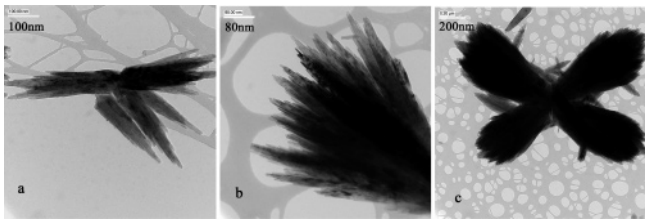

Figure 4. TEM images of rutile products of the reaction between H-titanate fibers prepared at various temperatures and 2.65 M HNO_3 at 80 °C. Image (a) is the product from the H-titanate fibers prepared by the hydrothermal treatment at T_h = 100 °C, image (b) is the product from the H-titanate fibers prepared T_h = 155 °C (b), and image (c) is the product from the fibers prepared at T_h = 200 °C.

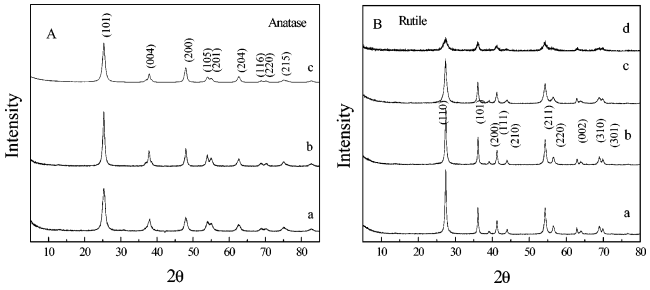

Figure 5. XRD patterns of anatase and rutile products from the H-titanate fibers by the phase conversion reactions. (A) Trace a is for anatase nanocrystals shown in Figure 3a, trace b is for anatase nanocrystals in Figure 3b, and trace c is for anatase nanocrystals in Figure 3c. (B) Trace a is for rutile nanocrystals shown in Figure 4a, trace b is for rutile nanocrystals in Figure 4b, trace c is for rutile nanocrystals in Figure 4c, and trace d is for the rutile crystals obtained by treating a H-titanate sample (prepared at T_h = 100 °C) with 2 M HNO_3 at 30 °C.

3.2. Reaction with Mineral Acids. The most distinguishing feature of the titanate nanofibers synthesized using this approach is their reactivity: both Na- and H-titanates react readily with mineral acids, yielding anatase or rutile nanocrystals (Figures 3 and 4), depending on the concentration of the acid. In a dilute (0.05 M) HNO_3 solution, we found that anatase was formed (Figure 5A), whereas, at a concentration above 2.0 M, the rutile phase was obtained (Figure 5B). The phase transition of the thin H-titanate fibers prepared at $T_h \leq 100$ °C (in Figure 1a) to anatase or rutile was observed to occur at temperatures as low as 30 °C. Actually, the titanate nanofibers synthesized at lower T_h transform to TiO_2 polymorphs at a lower temperature (T_c); on the other hand, the titanate nanofibers synthesized at T_h = 100, 155, and 200 °C were transformed to anatase or rutile in HNO_3 solutions (0.05 and 2.65 M) at 60, 80, and 120 °C, respectively. In general, the titanate fibers prepared at lower T_h were thinner and possessed a larger surface area, more defects (poorer crystallinity), and a less rigid crystal structure so that

(35) Chen, Q.; Du, G. H.; Zhang, S.; Peng, L. M. *Acta Crystallogr., Sect. B* **2002**, *58*, 587−593.
(36) Izawa, H.; Kikkawa, S.; Koizumi, M. *J. Phys. Chem.* **1982**, *86*, 5023−5026.

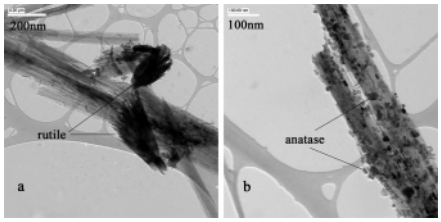

Figure 6. TEM images of intermediate products of the phase conversion reactions that H-titanate fibers reacted with 2.65 M HNO_3 at $T_c = 60$ °C (a), with 0.05 M HNO_3 at $T_c = 80$ °C (b). The H-titanate fibers were prepared by the hydrothermal treatment at $T_h = 155$ °C, and their image is shown in Figure 1b.

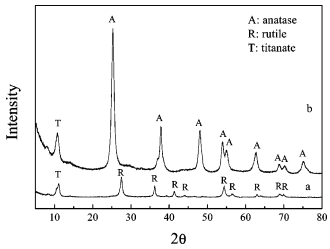

Figure 7. XRD patterns of intermediate products of the phase conversion reactions of H-titanate fibers reacted at $T_c = 60$ °C and 2.65 M HNO_3 (a), and at $T_c = 80$ °C and 0.05 M HNO_3 (b). H-titanate fibers prepared by the hydrothermal treatment $T_h = 155$ °C as shown in Figure 1b.

the phase change was easier. Therefore, we conclude that the H-titanate fibers with a high degree of crystallinity were more stable in acidic solutions.

We also found that the morphology of the anatase products was dependent on the parent titanate fibers. A TEM micrograph of the anatase product obtained from the thin titanate fibers at 80 °C is provided in Figure 3a. The product here was a monodispersed dispersion of crystals smaller than 10 nm. On the other hand, the anatase solids obtained from H-titanate fibers prepared at high temperature ($T_h = 200$ °C, in Figure 1c) were fibril aggregates of anatase nanocrystals, as is evident from the image provided in Figure 3c. In both cases, the reaction product retains the fibril morphology of the parent titanate fibers. Finally, the anatase product from transformation of the titanate fibers prepared at intermediate temperatures such as $T_h = 155$ °C (in Figure 1b) appears to be comprised of a combination of the above two cases, with both monodispersed anatase nanocrystals and fibril aggregates of the small anatase crystals.

A morphology of rutile product completely different from that of the parent H-titanate fibers was observed when the reaction of the parent fibers was undertaken at 2.65 M HNO_3. This is evident from the TEM images provided in Figure 4. This observation reveals that a radical structural reorganization took place during the reaction, which is clearly different from the phase transition from titanate to anatase.

To better understand the phase transitions, the reactions were also conducted with the same acid concentration at relatively low temperatures (i.e., $T = 60-80$ °C). The structure and morphology of the products obtained at these temperatures are summarized in the TEM images from Figure 6 and the XRD analysis in Figure 7. The resultant structures appear to be intermediates of an incomplete phase transition reaction. In these intermediate products, anatase or rutile phase coexists with the H-titanate but in different configurations. The coexistence of rutile crystals and titanate fibers in the intermediate resembles a mechanically blended mixture (Figure 6a). In contrast, within

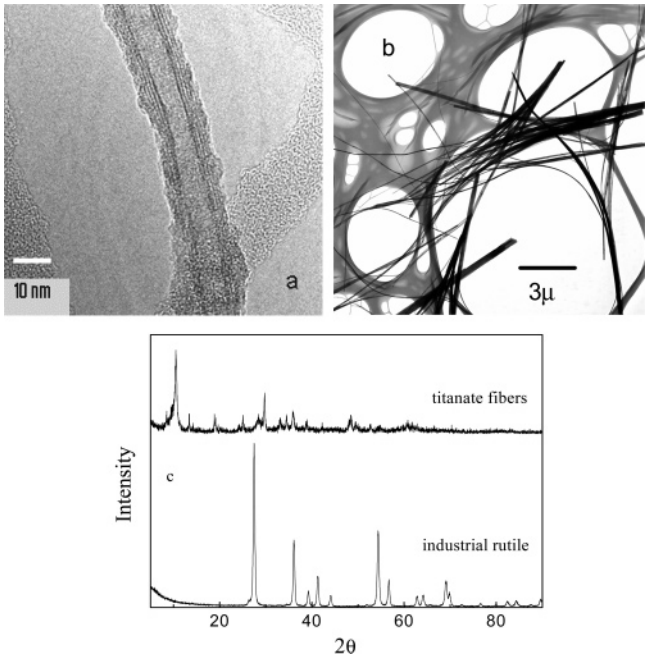

Figure 8. (a) The products of the backward reaction (from TiO_2 to titanate). A polycrystalline titanate nanotube obtained by the reaction between the rutile nanocrystals in Figure 4c and 10 M NaOH at 150 °C. The nanotube has an inner diameter of 3−4 nm and an outer diameter of ∼10 nm. (b) Titanate fibers prepared from an industrial material of 97% rutile and 10 M NaOH at 180 °C. (c) XRD patterns of the industrial rutile and product titanate prepared from the industrial rutile.

the intermediate phase transition to anatase, small anatase crystals of 10−20 nm over the outer surface of H-titanate fiber bundles are observed. This represents an interesting composite nanostructure of anatase crystals covered by titanate fibers (Figure 6b) and suggests that the titanate fibers convert to anatase crystals in situ, on the outer surface of the titanate fibers in a dilute acid solution. On the other hand, the rutile nanocrystals with thin rodlike morphology form from the concentrated acid solution (above 2.0 M) in which the parent titanate fibers are dissolved.

To our knowledge, this is the first report of the preparation of nanoscale particles of rutile from common inorganic salts at such low temperatures and low acid concentration. They are different from rutile nanorods or nanosized rutile particles prepared by the hydrolysis of $TiCl_4$ solution in the concentrated HNO_3 (15 M).[37,38] On the other hand, these fibers are relative stable against heat treatment, exhibiting mineral-like behavior. For instance, heating at 400−500 °C converts the H-titanate fibers prepared at $T_h \leq 100$ °C into anatase nanoparticles,[26,39] while the well-crystallized fibers prepared at 200 °C do not transform into anatase, even when exposed to temperatures as high as 650 °C. At temperatures above 900 °C, they were converted into rutile crystals.

3.3. Phase Transitions between Titanates and Titanium Dioxide Polymorphs. The titanium dioxide nanoparticles formed from titanate nanofibers can be converted back to sodium titanate by hydrothermal treatment with 10 M NaOH. We found that this reaction could take place at temperature as low as 60 °C. At 150 °C, the products are nanotubes (Figure 8a). Similar

(37) Huang, Q.; Gao, L. *Chem. Lett.* **2003**, *32*, 638−639.
(38) Cheng, H.; Ma, J.; Zhao, Z.; Qi, L. *Chem. Mater.* **1995**, *7*, 663−671.
(39) Tsai, C. C.; Hsisheng Teng, H. S. *Chem. Mater.* **2004**, *16*, 4352−4358.

Scheme 1. The Phase Transitions between Sodium- and Hydrogen-Titanates, Anatase, and Rutile by the Wet-Chemical Process

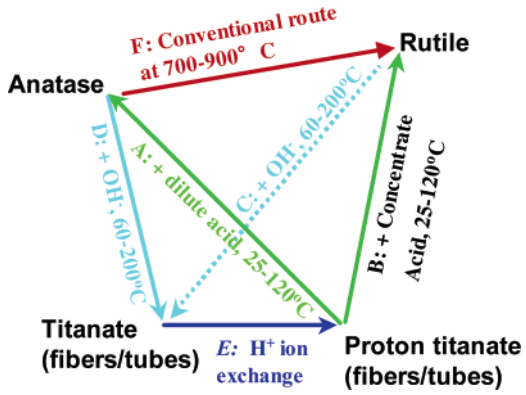

structures have been observed in the literature using titanium dioxides as raw materials.[18,21,22] Therefore, we can summarize the phase transitions between titanates and titanium dioxide polymorphs as shown in Scheme 1.

The phase transitions in Scheme 1 reveal that we can convert any phase of two titanium dioxide polymorphs and titanates into any other phase by the wet-chemical reactions at low temperatures (close to ambient). For example, rutile nanocrystals could be converted into anatase nanocrystals via sodium and protonated titanates (a route by reaction C → reaction E → reaction A). This is particularly noteworthy given that rutile is the most thermodynamically stable phase of titanium dioxide and that other TiO_2 phases eventually convert to rutile at high temperatures,[7,19] as indicated by reaction F in Scheme 1. However, reactive titanate nanoparticles can also be produced from rutile at relative low temperatures via the reaction with concentrate caustic soda (Scheme 1, reaction C). Anatase, a phase less stable than rutile, is readily produced from the titanate by reacting with dilute acid solution (Scheme 1, reactions E and A). Such phase transitions via simple wet chemistry reactions provide us opportunities to design and produce new materials with delicate nanostructures with great control. According to the phase transitions in Scheme 1, one can prepare nanostructures of anatase, rutile, and titanates from rutile powder via the wet-chemical process under moderate conditions. In addition, we found the size of the reactant particles in reactions C and D of Scheme 1 exerts considerable influence on the temperature of the phase transitions. For instance, coarse rutile particles were used as the reactant, and the phase transition to sodium titanate (reaction C) took place at the relatively higher temperature of ~170 °C. Figure 8b is an image of the titanate nanofibers prepared from an industrial starting material containing 97% rutile, which was used for the production of rutile pigment and kindly provided by Austpac Resources, Sydney, at 180 °C.

The XRD patterns of the reactant industrial rutile and the product titanate are illustrated in Figure 8c. There is no obvious diffraction peak of rutile observed in the titanate pattern. This suggests high purity of titanate nanofibers in the product. The reactive fibers can then be converted readily to nanostructures of anatase, rutile, and titanates. This reveals opportunities to produce these nanostructures directly from the raw mineral or industrial materials because rutile is the major form of TiO_2 minerals and industrial products.

Scheme 2. Structural Features of Hydrogen-Titanate (Top Left), Anatase (Top Right), and Rutile (Bottom Right), as Well as the Phase Transitions from the Hydrogen-Titanate to Anatase and Rutile, in Dilute and Concentrate Acid Solutions, Respectively

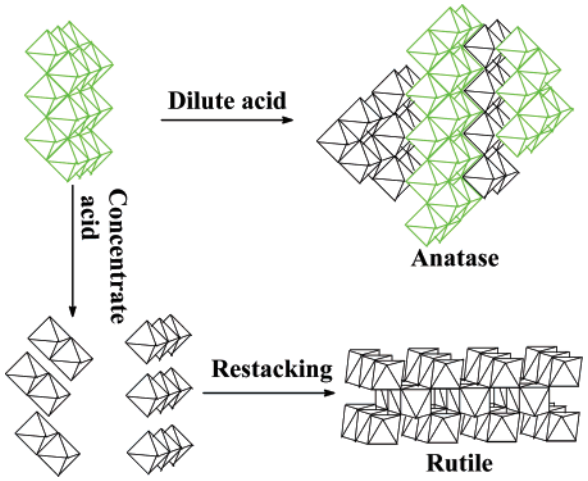

The anatase and rutile nanostructures clearly transform from the titanate nanofibers through different mechanisms. Whereas the product aggregates of anatase nanocrystals inherit their morphology from the reactant titanate fibers (Figure 3c), the rutile nanocrystals show no morphologial similarity to the initial titanate fibers. It is noted that the titanate and anatase have common structural features: both crystal lattices consist of the octahedra sharing four edges and the zigzag ribbons.[33,40,41] We propose that this is why the anatase nanocrystals form in situ on the parent titanate fibers as illustrated in Scheme 2. In the reaction with the acid, the H-titanate nanofibers dehydrate and the large structural units such as zigzag ribbons (green color in Scheme 2) remain relatively unchanged, rearranging to form anatase lattice. In contrast, each TiO_6 octahedron in rutile shares only two edges with others, and these edge-sharing octahedra form linear TiO_6 chains.[40] These chains link to each other by sharing vertices, resulting in three-dimensional lattices. Nevertheless, there exist no linear chains of two edge-sharing TiO_6 octahedra in the H-titanate nanofibers. Thus, the zigzag ribons of TiO_6 octahedra with four shared edges in H-titanate nanofibers have to be resolved into detached TiO_6 octahedra or their small clusters thereof to form the straight chains observed in rutile. The fact that the phase transition to rutile takes place at a high acid concentration (<2.0 M), as compared to 0.05 M for producing anatase, seems consistent with the proposal that the rutile lattice is reconstructed with the detached TiO_6 octahedra in solution as well as the observation that a more acidic environment is preferred for the formation of rutile phase.[42] Consequently, the morphology of the rutile crystals obtained from the titanate fibers shows no morphological resemblance to the fibers (Figure 4).

The ultraviolet and visible (UV/vis) spectra of the H-titanate fibers shown in Figure 1c, anatase fibril aggregate in Figure 3c, and rutile nanocrystals in Figure 4c are given Figure 9. The titanate fibers strongly absorb UV light with wavelength below 350 nm, while the anatase and rutile can absorb the light with

(40) Burdett, J. K.; Hughbanks, T.; Miller, G. J.; Richardson, J. W.; Smith, J. V. *J. Am. Chem. Soc.* **1987**, *109*, 3639−3646.
(41) Zheng, Y. Q.; Shi, E. W.; Li, W. J.; Chen, Z. Z.; Zhong, W. Z.; Hu, X. F. *Sci. China, Ser. E* **2002**, *45*, 120−129.
(42) Jolivet, J. P. *Metal Oxide Chemistry and Synthesis: From Solution to Solid State*; Wiley: West Sussex, 2003.

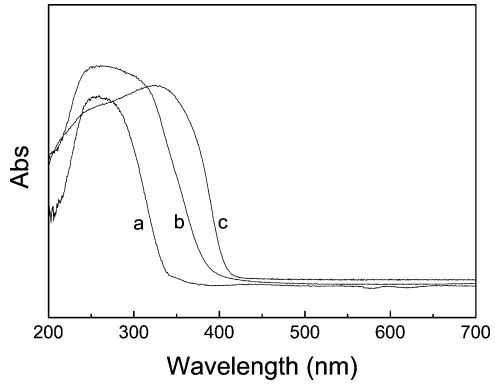

Figure 9. Ultraviolet and visible (UV/vis) spectra of the H-titanate fibers in Figure 1c (trace a), anatase fibril aggregate in Figure 3c (trace b), and rutile nanocrystals in Figure 4c (trace c).

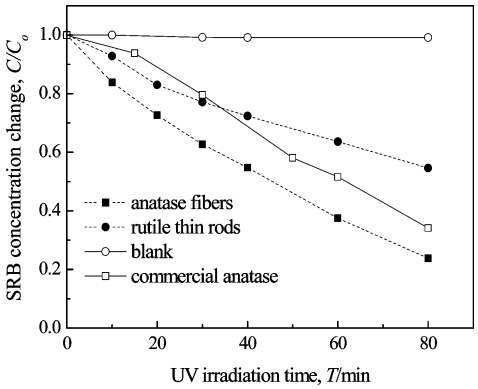

Figure 10. Photocatalytic activities of the samples: anatase fibril aggregate (Figure 3c) clusters of rutile thin rods (Figure 4c) and commercial anatase (particle sizes of 80−100 nm) for SRB degradation. The SRB concentration decreases with the reaction time. The catalyst concentration was 0.05 g/L, and the starting SRB concentration was 3×10^{-5} mol/L.

longer wavelength. This suggests that the H-titanate nanofibers are semiconductive solids but with a band gap substantially larger than those in the rutile and anatase estimated from the above spectra. The large band gap has an adverse effect on the catalytic performance when the materials are used as photocatalysts under UV light as discussed below, because a smaller amount of light will be absorbed.

3.4. Photocatalytic Performance. Both the anatase fibers and the rutile aggregates (Figure 3) prepared from titanate fibers are active photocatalysts for degradation of synthetic dyes under UV light irradiation as illustrated in Figure 10. The anatase fibers exhibit a better activity than the rutile, and both of them can be readily separated by filtration or sedimentation after reaction because of their morphologies. The parent titanate fibers exhibit a poor catalytic performance. The activity of commercial anatase with a particle size of 80−100 nm is also given in Figure 10 for comparison. The activity of the fibril anatase obtained in this study is higher than that of commercial anatase.

In addition to the photocatalytic activity, recovery of the catalyst from water when they are used in aqueous systems would seem to be a critical issue because the photocatalytic reaction takes place on the surface of the catalysts. Therefore, ultra-fine catalyst powders with a particle size of several nanometers (nm) should exhibit a superior activity because of the large surface-to-volume ratios. However, these ultra-fine powders could be very difficult to recover from water after they are used in aqueous systems, leading to a potential difficulty in

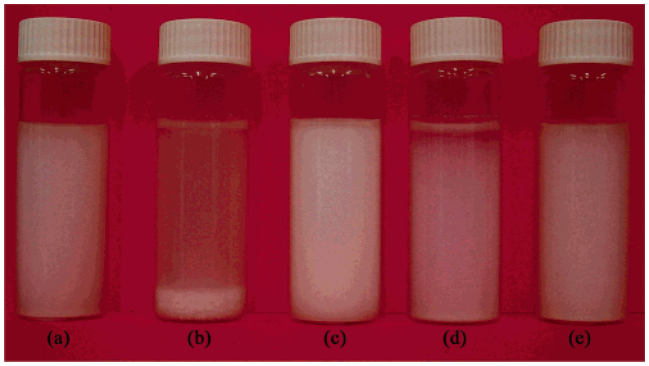

Figure 11. Sedimentation for 1 h in aqueous suspensions of H-titanate fibers (a), anatase fibril aggregate (b), commercial anatase (c, particle sizes of 80−100 nm), commercial P25 (d), and clusters of rutile thin rods (e) (concentration: 0.6 g/L, ultrasonic treatment for 20 min).

downstream separation. In fact, the high cost for separating the catalyst nanocrystals has seriously impeded the applications of TiO_2 photocatalysts at industrial scale.[43,44] Continuing efforts has been made to synthesize the TiO_2 structures that can be separated readily and have the superior performance of anatase nanocrystals.[44,45] In the present study, we found that fibril aggregate of anatase, obtained from titanate fibers and with lengths at scale of micrometers as illustrated in Figure 3, can be readily separated from fluid by filtration or sedimentation. As shown in Figure 11, the anatase fibril aggregates sedimentated from an aqueous suspension in less than 1 h, while the aqueous suspensions of a commercial anatase powder and P25 (a mixture powder of ∼80% anatase and ∼20% rutile, provided by Degussa, Germany) were unclear after an hour. The rutile samples obtained from the titanate fibers are clusters of thin rods, which also take long time to sedimentate down from the aqueous suspension. The fact that the fibril photocatalysts can be readily recovered by sedimentation is of great significance for their potential application as photocatalysts for the elimination of organic pollutants from water at an industrial scale. This important environmental application has been seriously impeded by the high cost of recovering the catalyst nanocrystals.[43] Finally, we note the apparently significant potential for recyclable TiO_2 photocatalysts with superior chemical activity in applications such as odor elimination from drinking water, degradation of oil spills in surface water systems, and degradation of harmful organic contaminants such as herbicides, pesticides, and refractive dyes.

IV. Conclusion

Titanate nanofibers of various sizes and layered structure were prepared from inorganic titanium compounds by hydrothermal reactions. Possessing a very large surface area-to-volume ratio, these nanostructures of titanate and TiO_2 polymorphs are different from "refractory" mineral substances and exhibit a high reactivity. Phase transitions between the nanostructures of titanate and TiO_2 polymorphs take place readily in simple wet-chemical processes at temperatures close to ambient temperature. This is highly significant because it allows us to fabricate

(43) Hoffmann, M. R.; Martin, S. T.; Choi, W.; Bahnemannt, D. W. *Chem. Rev.* **1995**, *95*, 69−96.
(44) Beydoun, D.; Amal, R.; Low, G. K.-C.; McEvoy, S. *J. Phys. Chem. B* **2000**, *104*, 4387−4393.
(45) Zhu, H. Y.; Orthman, J.; Li, J.-Y.; Zhao, J.-C.; Churchman, G. J.; Vansant, E. F. *Chem. Mater*. **2002**, *14*, 5037−5044.

delicate new nanostructures of titanium dioxides and titanates by appropriate engineering of these wet-chemical reactions. The phase transition phenomenon is likely of remarkable interest to the scientists in areas of materials science,[1−6] photocatalysis using titania catalysts,[7−9,18] clinical titanium implant devices,[46] and corrosion of titanium material.[47,48] The fact that we can synthesize nanostructures of titanate and TiO_2 directly from rutile minerals and related industrial-grade reactants by a new scheme of hydrometallurgical reactions highlights the application potential of the reported phase transitions. This study indicates that the reaction of nanoparticulates offers an effective approach to preparation of inorganic oxide nanocrystallites with desirable morphologies. Finally, we have demonstrated that the morphology of the anatase nanocrystal aggregates plays a crucial role in their potential applications as photocatalysts.

(46) Kim, H. M.; Miyaji, F.; Kokubo, T.; Nakamura, T. *J. Biomed. Mater. Res.* **1996**, *32*, 409−417.
(47) Michaelis, A.; Kudelka, S.; Schultze, J. W. *Corros. Rev.* **2000**, *18*, 395−423.
(48) Bearinger, J. P.; Orme, C. A.; Gilbert, J. L. *Surf. Sci.* **2001**, *491*, 370−387.

Acknowledgment. Financial support from the Australian Research Council (ARC), the 973 Program (2002CB211800 and 2003CB415006), Key Project of CME (03047), SRFDP (20020055007), NSFC (90206043 and 50221201), and NCET (040219) of China is gratefully acknowledged. H.Y.Z. is indebted to the ARC for a QE II Fellowship. We thank Ms Y. Q. Bai for conducting part of the TEM measurement. Facilities as well as scientific and technical assistances from the staffs in the NANO Major National Research Facility at the Electron Microscope Unit, the University of Sydney, are gratefully acknowledged.

JA044689+